Structure and phase transition in $BaThO_3$: A combined neutron and synchrotron X-ray diffraction study

Gabriel L. Murphy,[1,2] Brendan J. Kennedy,[1,*] Zhaoming Zhang,[2] Maxim Avdeev,[2] Helen E A. Brand,[3] Philip Kegler [4] and Evgeny V. Alekseev [4,5]

[1] *School of Chemistry, The University of Sydney, Sydney, NSW 2006, Australia*

[2] *Australian Nuclear Science and Technology Organisation, Lucas Heights, NSW 2234, Australia*

[3] *Australian Synchrotron, 800 Blackburn Road, Clayton, Victoria 3168, Australia*

[4] *Institute of Energy and Climate Research (IEK-6), Forschungszentrum Jülich GmbH, 52428 Jülich, Germany*

[5] *Institute für Kristallographie, RWTH Aachen University, 52066 Aachen, Germany*

*corresponding author: Brendan.Kennedy@Sydney.edu.au

Abstract

The structure of $BaThO_3$, obtained by solid state synthesis, was refined for the first time by the Rietveld method using a combination of synchrotron X-ray and neutron powder diffraction data. $BaThO_3$ has an orthorhombic structure at room temperature, in space group *Pbnm* with a = 6.3491(5), b = 6.3796(4) and c = 8.9907(7) Å. Heating $BaThO_3$ to above 700 °C results in a continuous transition to a second orthorhombic structure, in space group *Ibmm*, demonstrated by both *in situ* neutron and synchrotron X-ray powder diffraction measurements. The coefficient of volumetric thermal expansion for $BaThO_3$ is determined to be 1.04 x 10^{-5} $^{o}C^{-1}$ from 50 to 625 ^{o}C (*Pbnm* phase), and 9.43 x 10^{-6} $^{o}C^{-1}$ from 800 to 1000 ^{o}C (*Ibmm* phase). $BaThO_3$ was found to decompose upon exposure to atmospheric moisture resulting in the formation of ThO_2. The thermal expansion of ThO_2, which invariably co-exists with $BaThO_3$, is also described.

Key Words: Barium Thorium Oxide; Perovskite; Phase Transition; Neutron Diffraction; Synchrotron X-ray Diffraction.

Introduction

The stability and properties of actinide oxides are of interest in optimising the utilisation of mixed oxide nuclear fuels as well as in the management and storage of spent nuclear fuel [1]. That uranium can adopt a range of oxidation states (typically 4, 5 or 6 in oxides) and coordination environments (coordination number 6-8) makes it attractive to solid state chemists and a sizeable body of information on the crystal chemistry of uranium oxides now exists [2, 3]. In comparison thorium is only found in the tetravalent state in oxides. This, coupled with the relative technological importance of U compared with Th, has resulted in considerably less interest in the crystal chemistry of Th oxides [4]. Whilst both U and Th are radioactive they can be readily handled with appropriate care; the same cannot be said for the heavier actinides all of which require demanding safety procedures. Understanding the structural behaviour of the heavier actinides is important, since these will constitute a significant proportion of high level active waste (HLW) from spent nuclear fuel. Consequently Th and U often serve as surrogates for the structural behaviour of heavier actinides despite the subtle differences in their chemistry.

Considering U(IV) and Th(IV) are expected to be markedly different from each other in condensed phases, through the presence of 5*f* electrons in the former and absence in the latter, it is pertinent to consider the crystal chemistry of ternary thorium oxide phases. Thorium is most commonly encountered as ThO_2 and there are reports that this reacts with $BaCO_3$ at high temperatures to form $BaThO_3$ [5, 6]. Under similar conditions $BaUO_4$ forms, although reduction of this can yield $BaUO_3$ [7, 8]. Both $BaThO_3$ and $BaUO_3$ are described as adopting a perovskite structure, with $BaThO_3$ reported either as cubic in space group $Pm\bar{3}m$ or orthorhombic (although no space group was assigned)[5, 6]. Establishing the appropriate space group for perovskites requires examination of both the splitting of the main Bragg reflections and the nature of any superlattice reflections that may arise due to tilting of the corner sharing octahedra. For $BaThO_3$ the X-ray diffraction superlattice reflections are expected to be extremely weak, and the modest peak shape resolution of laboratory powder

X-ray diffractometers is often inadequate in detecting the splitting of the main Bragg reflections.

Unlike most ABO_3 perovskites there is evidence that $BaThO_3$ decomposes on exposure to the atmosphere[9, 10]. This together with the radioactivity of Th has been a barrier to detailed structural analysis of $BaThO_3$. $BaThO_3$ has been the subject of a number of computational studies[11, 12] and recently Lebedev [13] predicted, using first-principles density functional theory (DFT), that the orthorhombic structure of $BaThO_3$, in space group *Pbnm*, will be the most stable and that a second orthorhombic form in *Ibmm* (described in the alternate setting of *Imma*) is close in energy. These two orthorhombic structures differ in terms of the nature of the cooperative tilting of the ThO_6 octahedra. The *Pbnm* structure is described as $a^-a^-c^+$ in Glazer's [14] notation having in-phase tilting about [001] and out-of-phase tilting about [110]. The tilt system in *Ibmm* is $a^-a^-c^0$ indicating that there is no tilting about [001]. Both structures are described by a $\sqrt{2} \times \sqrt{2} \times 2$ superstructure of the ~ 4 Å $Pm\bar{3}m$ parent structure and the transition between them is allowed, by group theory, to be continuous [15].

Given the relatively small energy difference between the *Pbnm* and *Ibmm* structures Lebedev [13] asserted that a second order *Pbnm* - *Ibmm* transition would occur at a temperature slightly above room temperature , although there is no experimental evidence to support this. Indeed earlier heat capacity measurements by Krishnan *et al.* [16] showed no evidence for such a transition below 547 ^oC. Lebedev[13] postulated that this was a consequence of sample purity, although he did not hypothesise how impurities would impact on the transition. It is well established that chemical doping can alter the relative stability of the *Pbnm* and *Ibmm* phases and can be used to tune the temperature at which a transition between them occurs [17, 18]. The tolerance factor for $BaThO_3$, defined as $t = \frac{r_A + r_O}{\sqrt{2}(r_B + r_O)}$ where r_A, r_B and r_O are the ionic radii of the Ba^{2+}, Th^{4+} and O^{2-} ions, is 0.910. By comparison with other well studied perovskites, such as $SrZrO_3$ with t = 0.947 [19], $SrRuO_3$ with t = 0.994[20] or $SrTcO_3$ with t = 0.982 [21 22], that exhibit a thermally induced *Pbnm*- *Ibmm* transition, it is reasonable to propose that if the *Pbnm* - *Ibmm* transition occurs in $BaThO_3$ it will occur at temperatures well above room temperature.

There is interest in establishing the structural and thermal behaviour of U and Th oxides particularly in relation to spent fuel and waste forms resulting from future thorium reactors [23]. As part of our current interest in U and Th oxides [8, 24-26] we have undertaken an

in-situ variable temperature structural study of $BaThO_3$ using high-resolution synchrotron X-ray and neutron powder diffraction methods. These measurements demonstrate for the first time experimentally that the *Pbnm* - *Ibmm* transition does occur but at a much higher temperature than that postulated by Lebedev[13].

Experimental

Caution. Thorium predominantly decays by α emission (4.083 MeV) with a half-life of 1.405 x 10^{10} years where the first progeny, Ra-228, decays by β emission (0.017 Mev) with a half-life of 5.8 years Appropriate radioactive material handling precautions must be taken with thorium.

Synthesis

$BaThO_3$ was prepared through a solid state method in which excess $BaCO_3$ (with the intention of it acting as a flux) was mixed with ThO_2. ThO_2 was obtained from sintering high purity thorium metal supplied by ANSTO Minerals, Lucas Heights, Australia. All necessary precautions were taken when handling radioactive thorium materials. The powder mixture was compacted into a pellet and heated to 1250 ^oC in air for 80 hours with intermittent mixing. X-ray diffraction (XRD) measurements were taken using a Bruker D8 advance diffractometer with Cu K_α radiation at room temperature to monitor the generation of $BaThO_3$. Attempts to prepare $SrThO_3$ using similar solid state methods as those used for $BaThO_3$ or by high temperature/high pressure (4 GPa 900-1400 ^oC) methods using a Voggenreiter LP 1000-540/50 instrument installed at IEK-6, Forschungszentrum Jülich, were unsuccessful, with ThO_2 invariably being recovered (consistent with $SrThO_3$ having a positive energy of formation as predicted by first-principles calculations[27]).

Analysis

Synchrotron X-ray powder diffraction (S-XRD) data were collected using the powder diffractometer at the beamline BL-10 of the Australian Synchrotron [28]. The sample was finely ground and housed in a sealed 0.2 mm diameter quartz capillary that was rotated during the measurement. The wavelength was set at ~ 0.775 Å, and the precise value of this was determined using a NIST LaB_6 standard reference material to be 0.774506 Å. Data were collected from RT to 1000 ^oC at a heating rate of 5 ^oC /min using a Cyberstar hot-air blower. Neutron powder diffraction (NPD) data were measured by the high-resolution powder diffractometer Echidna at ANSTO's OPAL reactor, using a wavelength of 1.622 Å [29]. The

sample was compacted into a pellet and placed in a cylindrical vanadium can which was mounted in an ILL type high vacuum furnace employing niobium elements and operating at $< 10^{-6}$ torr. The sample container was not sealed during these measurements, such that the sample was exposed to the vacuum. The temperature was increased at 10 °C /min from RT to 1000 °C and data collected incrementally. The structures described here were refined by the Rietveld method as implemented in the program GSAS/EXPGUI[30, 31]. The peak shapes were modelled using a pseudo-Voigt function and the background was estimated using a 12-18 term shifted Chebyschev function. The scale factor, detector zero point, lattice parameters, atomic coordinates and atomic displacement parameters were refined together with the peak profile parameters.

Thermogravimetric analysis (TGA) and differential scanning calorimetry (DSC) measurements were obtained using an SDT Q600 TGA from 25 to 600 ^{o}C using a constant air flow. The samples were contained in quartz crucibles and measurements were obtained at heating rates of 5 ^{o}C /min. Measurements were conducted on $BaThO_3$ immediately after synthesis and also after prolonged exposure to the atmosphere.

Results and Discussion

X-ray diffraction patterns of the $BaThO_3$ samples showed these invariably contained ThO_2, consistent with the observations of previous studies[5, 6, 10], with the amount of this increasing upon prolonged exposure of the powder sample to the atmosphere. The amount of ThO_2 could be reduced somewhat by the use of excess $BaCO_3$ in the reaction mixture acting as a flux, this method was shown to be successful in previous studies[10] . Rietveld refinement against the S-XRD data showed that the sample studied here contained 13.53(33) wt% of ThO_2. No reflections due to crystalline barium oxides or carbonates were apparent in the diffraction patterns.

Whilst Nakamura [5] established that $BaThO_3$ is orthorhombic, using a conventional X-ray source, the space group and structural details were not determined. Orthorhombic symmetry is consistent with the low Goldschmidt tolerance factor of $BaThO_3$ (t = 0.910). Oxides with such low tolerance factors require cooperative tilting of the corner sharing ThO_6 octahedra, lowering the symmetry from cubic, to stabilise a perovskite type structure [15]. Our synchrotron X-ray diffraction data suggest the space group to be *Pbnm* through the observation of diagnostic splitting of Bragg reflections indicative of orthorhombic symmetry

and of weak, but characteristic, superlattice reflections. The combination of resolved peak splitting and the presence of superlattice reflections enabled precise determination of the lattice parameters and atomic coordinates.

It is pertinent to comment on the superlattice reflections in $BaThO_3$. For ABO_3 perovskites these are generally associated with the tilting of the octahedra, with *R*-point (k = ½ ½ ½) softening of the Brillouin zone associated with out-of-phase tilting of the octahedra and *M*-point (k = ½ ½ 0) softening with in-phase tilting. *X*-point reflections (k = 0 0 ½) require the presence of both *R*-point and *M*-point reflections, however these also gain intensity from the displacement of the *A*-site cation from the equivalent (0, ½, ¼) position. In the present case the displacement of the Ba cation is the major contributor to the intensity of the *X*-point reflections. Consequently whilst X-ray diffraction data are relatively insensitive to the displacement of the lighter anions, the *X*-point reflections have appreciable intensity in *Pbnm* and are space group forbidden in *Ibmm*, and are thus sensitive to a transition between these. The two strongest *X*-point reflections are the 021 reflection at 2θ = 14.79 ° (d = 3.007 Å) and 113 at 2θ = 17.85 ° (d = 2.496 Å), and these are noticeably stronger than the two strongest *M*-point superlattice reflections: 120 reflection at 2θ = 15.61 ° (d = 2.851 Å) and 122 at 2θ = 18.50 ° (d = 2.408 Å). The *R*-point 121 reflection has intensity intermediate between these, see Figure 1. Ultimately the orthorhombic structure was confirmed using NPD. Refinement of the structure against the NPD set, illustrated in Figure 2, provides accurate and precise atomic coordinates for anions and these are given in Table 1. The structures of both the *Pbnm* and *Ibmm* forms of $BaThO_3$ are shown in Figure 3 where the differences in the octahedra tilting are illustrated. The lattice parameters refined against the data recorded at room temperature a = 6.3491(5), b = 6.3796(4), c = 8.9907(7) Å are in good agreement with the values calculated for $BaThO_3$ by Lebedev [13], a = 6.345(2), b = 6.376(2) and c = 8.992(2) Å, although the differences between the refined and calculated atomic coordinates are larger.

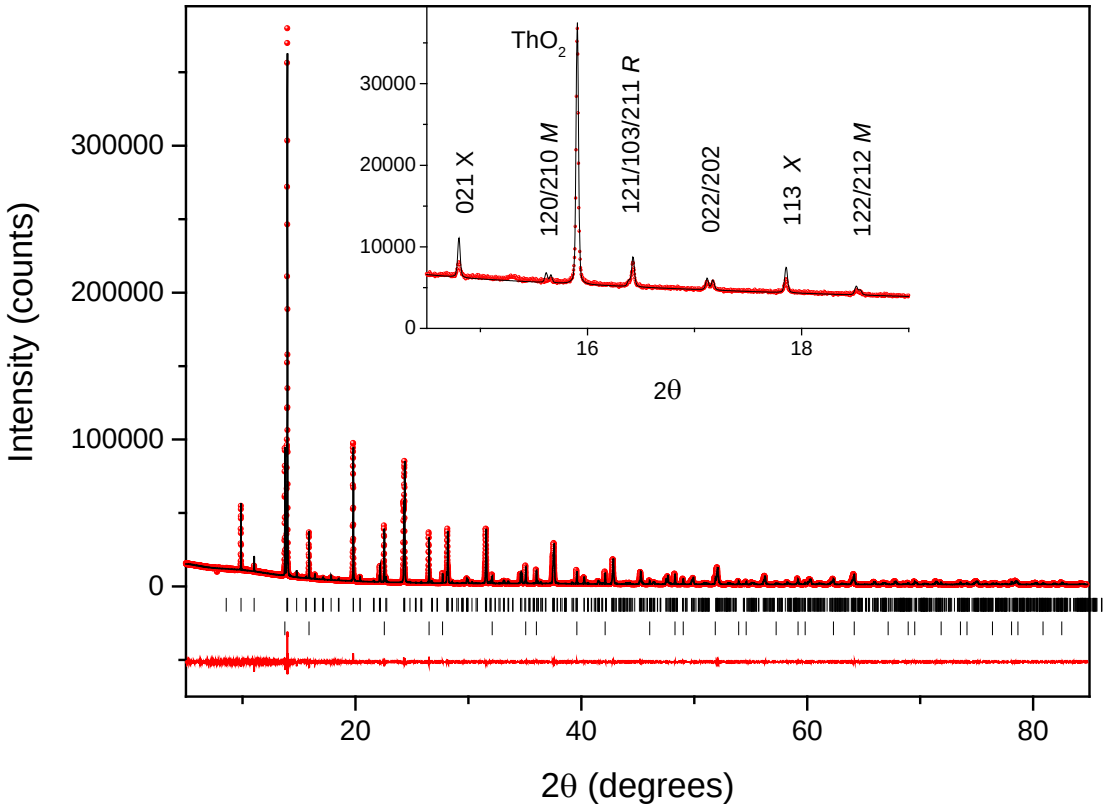

Figure 1. Observed, calculated and difference S-XRD profiles for $BaThO_3$ at room temperature. The upper set of tick marks show the positions of the space group allowed reflections for the *Pbnm* phase and the lower tick marks are for the ThO_2 impurity phase in $Fm\bar{3}m$. The inset highlights the presence of superlattice reflections associated with tilting of the ThO_6 octahedra in $BaThO_3$.

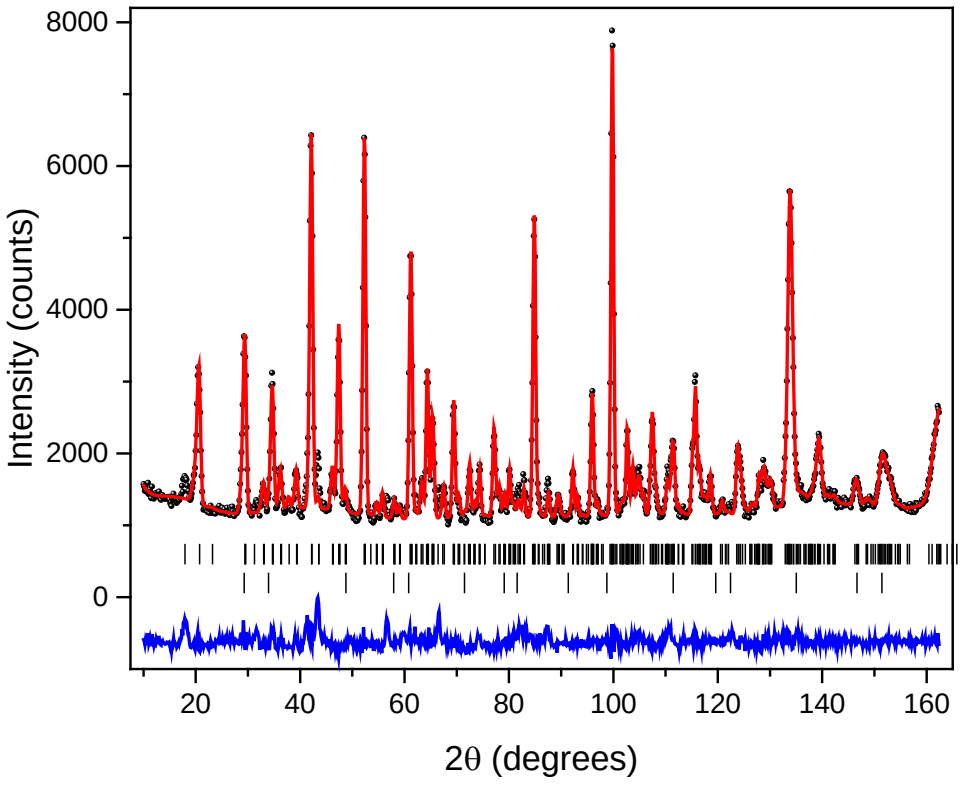

Figure 2. Observed, calculated and difference NPD profiles for $BaThO_3$ at room temperature. The upper set of tick marks show the positions of the space group allowed reflections for the *Pbnm* phase and the lower tick marks are for the ThO_2 impurity phase. The unfitted intensity near $2\theta = 19°$ is from an unknown impurity phase and was lost upon heating and did not reappear on cooling.

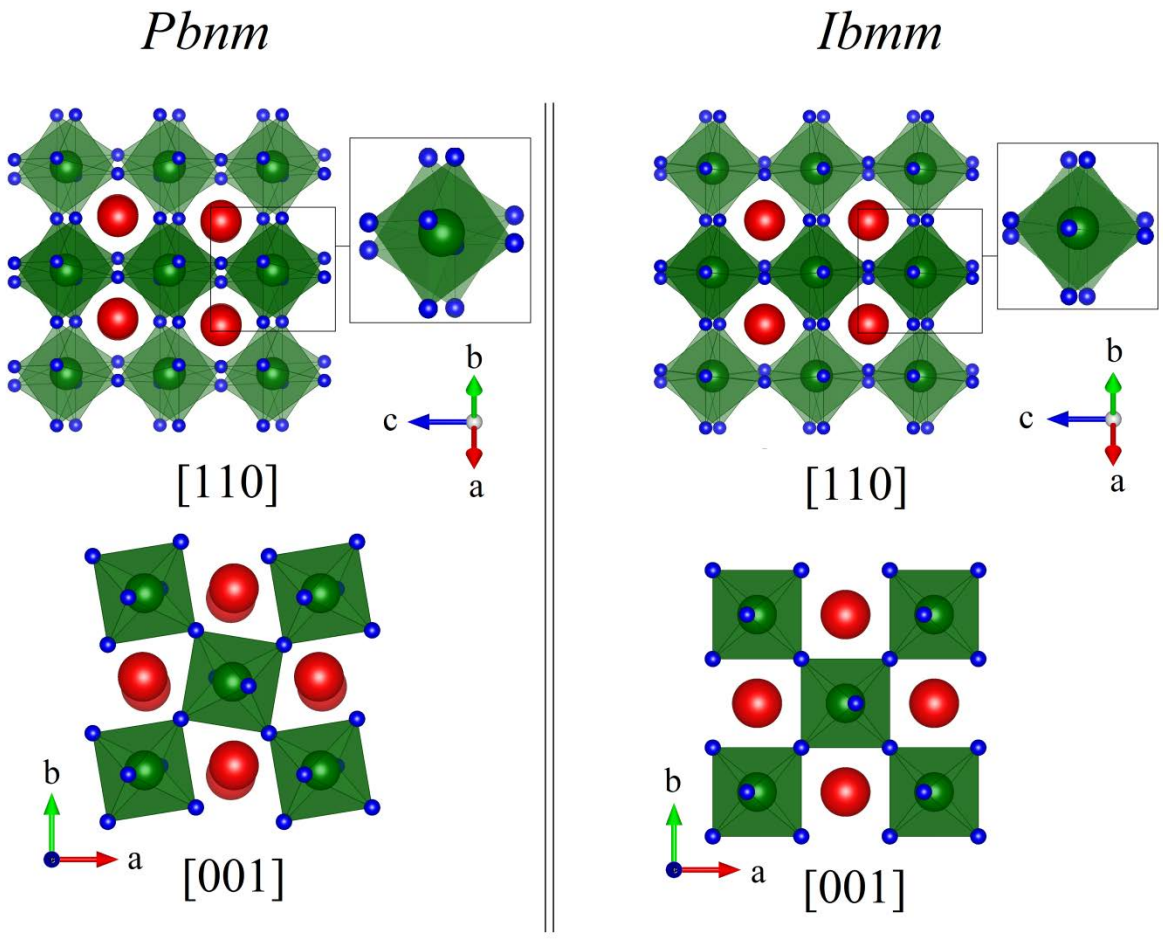

Figure 3. Representations of the *Pbnm* and *Ibmm* variants of $BaThO_3$, green, red and blue spheres respectiveily represent thorium, barium and oxygen, ThO_6 octahedra are shown as green octahedra. The *Pbnm* to *Ibmm* transition involves the loss of the in-phase cooperative tilting of the ThO_6 around the [001] axis, while the out-of-phase tilt about the [110] direction is present in both structures (the inset highlights the larger out-of-phase tilt angle at RT in *Pbnm* than at 1000ºC in *Ibmm*).

Table 1

Crystallographic parameters for $BaThO_3$ at RT and 1000 ºC refined against neutron powder diffraction data. The structures are described in space group *Pbnm* and *Ibmm* at the lower and higher temperatures respectively.

Structural parameters		RT	1000 ºC
Space Group		*Pbnm*	*Ibmm*
Lattice Parameters/Å	*a*	6.3491(5)	6.4222(10)
	b	6.3796(4)	6.4330(12)
	c	8.9907(7)	9.0995(17)
Unit cell volume/Å^3		364.16(5)	375.94(12)
Ba	*x*	0.0109(20))	-0.006(15)
	y	0.5298(8)	0.5
	z	0.25	0.25
	$100u_{iso}$/Å^2	0.29(11)	4.92(31)
Th	*x*	0.0	0.0
	y	0.0	0.0
	z	0.0	0.0
	$100u_{iso}$/Å^2	0.32(4)	2.14(7)
O1	*x*	-0.0913(16)	-0.037(11)
	y	-0.0237(15)	0
	z	0.25	0.25
	$100u_{11}$/Å^2	0.95(43)	12.5(7)
	$100u_{22}$/Å^2	2.75(48)	18.5(6)
	$100u_{33}$/Å^2	1.09(49)	1.6(13)
	$100u_{12}$/Å^2	1.56(38)	0
	$100u_{eq}$/Å^2	1.60	10.8
O2	*x*	0.2073(10)	0.25
	y	0.2905(10)	0.25
	z	0.0457(7)	0.0421(26)
	$100u_{11}$/Å^2	1.44(25)	7.2(16)
	$100u_{22}$/Å^2	1.28(25)	6.5(18)
	$100u_{33}$/Å^2	1.14(26)	10.1(11)
	$100u_{12}$/Å^2	-0.74(26)	-3.4(11)
	$100u_{13}$/Å^2	0.38(19)	0
	$100u_{23}$/Å^2/	-0.25(20)	0
	$100u_{eq}$/Å^2	1.29	7.95

Pbnm. Ba, O1: 4*c*; Th: 4*a*; O2: 8*d*
Ibmm. Ba, O1: 4*e*; Th: 4*a*; O2: 8g
RT refinement: Rp = 0.036, Rwp = 0.053, χ^2 = 4.53 for 44 variables
1000 ºC refinement: Rp = 0.040, Rwp = 0.055, χ^2 = 5.93 for 35 variables

Table 2 Selected bond lengths for $BaThO_3$ in space group *Pbnm* at RT and *Ibmm* at 1000 ºC obtained from refinement against neutron powder diffraction data.

Cation	Anion	Bond length@ RT /Å	Bond length @ 1000 ºC /Å
Ba	O1	2.921(11)	2.93(7)
	O1	2.686(17)	3.226(13) x 2
	O2	2.695(9) x 2	3.48(4) x 4
	O2	3.056(10) x2	
	O2	3.210(9)x 2	2.97(5) x 2
Th	O1	2.3261(28) x 2	2.290(7) x 2
	O2	2.310(6) x 2	2.302(4) x 4
	O2	2.326(6) x 2	

Heating the sample to above 700 °C resulted in the loss of the *X*-point reflections in the S-XRD profiles, at the same time the *M*-point reflections are also lost. At 725 °C there is still evidence for intensity associated with the *R*-point reflection and it appears that the sample has transitioned to *Ibmm* near 700 °C, see Figure 4. These observations were confirmed using NPD data collected at wider temperature intervals. Unfortunately the errors in the intensities of the *R*-point reflection are relatively large, reflecting (i) that these gains intensity from the displacement of the anions in the structure and (ii) they sit on "top" of the strongly structured background associated with the capillary. This combination means it is not possible to extract accurate intensities necessary to confirm if the transition is second order. Accordingly the structures were refined using space group *Pbnm* for data collected at or below 700 °C and in *Ibmm* for temperatures above this. Figure 5 summarises the temperature dependence of the unit cell parameters and cell volume.

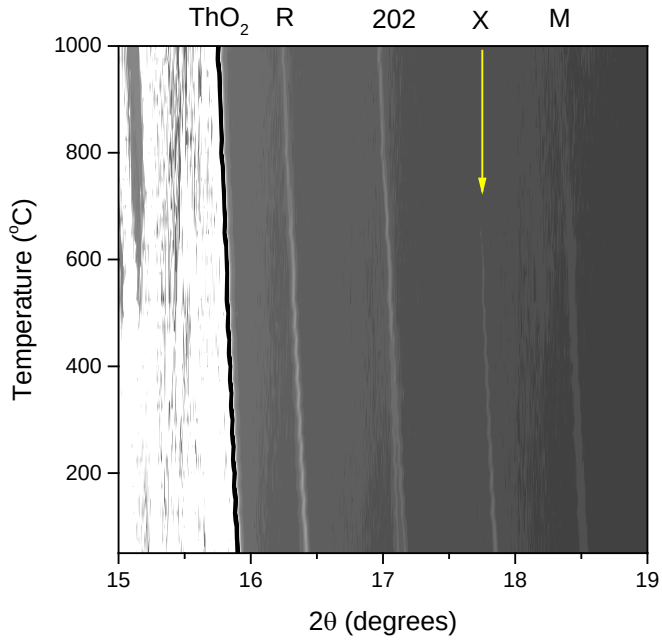

Figure 4. Temperature dependence of a portion of the S-XRD profiles for $BaThO_3$ illustrating the loss of the X-point 113 reflection near 700 °C. The textured background is due to the quartz capillary.

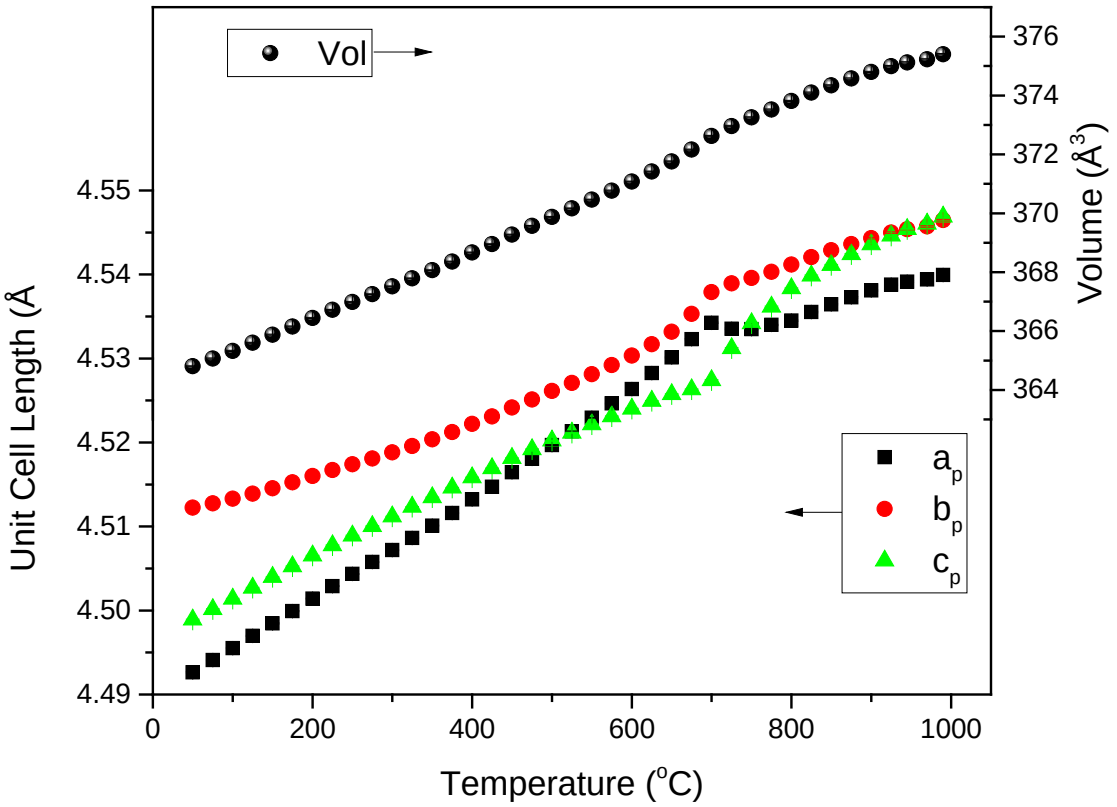

Figure 5. Temperature dependence of the unit cell volume and equivalent primitive unit cell parameters ($a = \sqrt{2}a_p;\ b = \sqrt{2}b_p;\ c = 2c_p$) for $BaThO_3$ deduced from Rietveld refinements of synchrotron X-ray diffraction data. The anisotropic change in the unit cell parameters around 700 °C is a consequence of the *Pbnm -Ibmm* transition.

Whilst it can be difficult to estimate the precise temperature of a continuous phase transition from diffraction data, the loss of the tilts in $BaThO_3$ near 700 °C results in a dramatic change in the anisotropic thermal expansion of the cell, with the thermal expansion of the *a*-parameter being weakly negative. Similar anomalies have been observed in other perovskites including $SrZrO_3$, $SrTcO_3$ and $SrRuO_3$ [19, 20, 22]. The volume vs temperature curve in Fig. 5 shows positive thermal expansion with a slight change in slope at the temperature of the *Pbnm – Ibmm* phase transition, with the high-temperature phase having a lower thermal expansion than the low-temperature phase. Evidently a volume strain is introduced by the transition. The linear thermal expansion coefficients (TEC) for the two phases were

estimated as $\alpha_i = \frac{(a_{High} - a_{low})}{a_{High} * \Delta T}$, where i is the unit cell direction and ΔT the change in temperature, and given in Table 3. The volumetric TEC $\bar{\alpha}$ was calculated in a similar manner using the cube root of the volume. Negative thermal expansion has been observed in the thorium oxy-phosphate $Th_2O(PO_4)_4$ [32] as well as in a number of perovskite related structures [33] however the thermal expansion of $BaThO_3$ is unexceptional.

Table 3 Linear and volumetric thermal expansion coefficients for $BaThO_3$ in space groups *Pbnm* and *Ibmm.*

	Pbnm (50-625 °C)	*Ibmm* (800-1000 °C)
α_a ($^oC^{-1}$)	1.37 x 10^{-5}	7.35 x 10^{-6}
α_b ($^oC^{-1}$)	7.46 x 10^{-6}	8.40 x 10^{-6}
α_c ($^oC^{-1}$)	1.00 x 10^{-5}	1.25 x 10^{-5}
$\bar{\alpha}$ ($^oC^{-1}$)	1.04 x 10^{-5}	9.43 x 10^{-6}

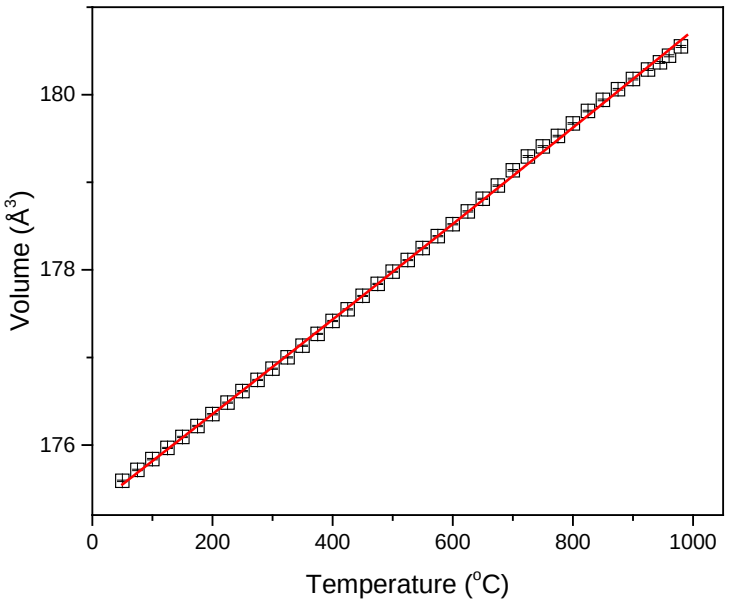

Figure 6. Temperature dependence of the unit cell volume for the cubic ThO_2 phase present in the $BaThO_3$ sample.

The presence of some ThO_2 in the sample provided information on the thermal expansion behaviour of this. An unexpected observation of this is the very small anomaly around 700 °C; that is near the phase transition of the major $BaThO_3$ phase, see Figure 6. It appears that the strain associated with the *Pbnm* - *Ibmm* transition in $BaThO_3$ is reflected in the thermal expansion of the ThO_2 impurity phase. The average linear TEC $\bar{\alpha}$ for ThO_2 is derived as 1.01 x 10^{-5} $^oC^{-1}$, in reasonable agreement with the earlier studies [34, 35] and are similar to values reported for other fluorite type materials [36].

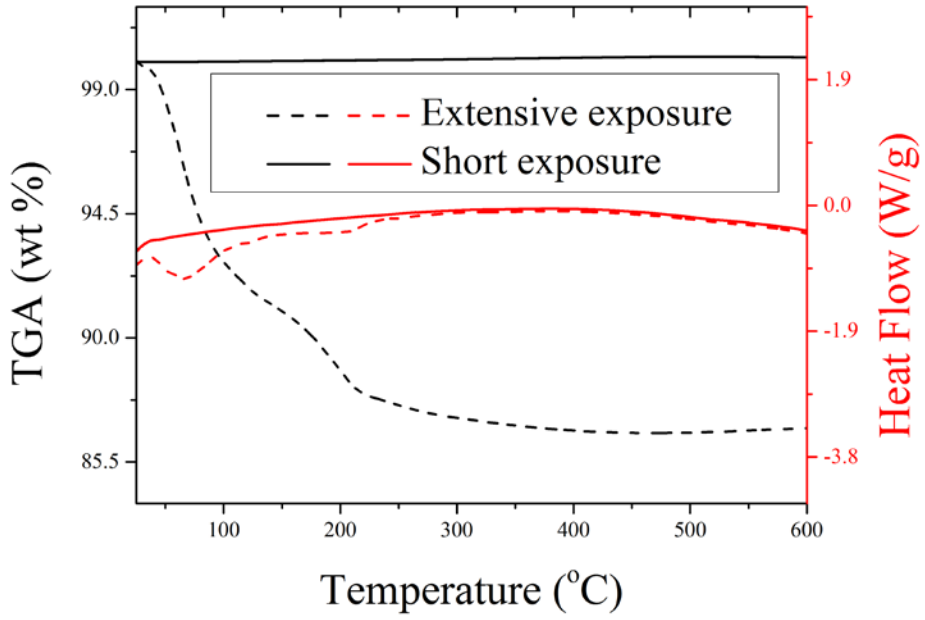

Figure 7. TGA (black) and DSC (red) measurements for freshly prepared (solid lines) and aged (dashed lines) samples of $BaThO_3$ at 5 ^oC/min in air.

NPD measurements taken after a sample of $BaThO_3$ had been exposed to the normal laboratory atmosphere for several days showed a noticeable increase in background, indicative of incoherent scattering suggesting the presence of hydrogen. Previous studies have suggested that the instability of $BaThO_3$ is a consequence of reacting with either moisture or CO_2.[9, 10, 16, 37] That this is associated with the absorption of moisture from the atmosphere was also established using a combination of thermogravimetric analysis and differential scanning calorimetry (TGA/DSC), Figure 7. Measurements were taken on a sample immediately after synthesis and again after several days of exposure to the atmosphere. The exposed sample displayed an approximate 14 wt% loss on heating between 50 ^oC and approximately 300 ^oC. In contrast there was no significant weight loss in the

freshly prepared sample. The DSC showed two endothermic events at approximately 80 and 200 ^{o}C for the aged sample. The former is from the loss of physisorbed surface water/moisture, whereas the second, at temperature above that of the boiling point of water, is due to chemisorbed water. The NPD diffraction pattern of the exposed sample showed a significant increase in the intensity of the peaks from ThO_2 and a concurrent reduction in the intensity of the $BaThO_3$ Bragg reflections. That $BaThO_3$ is unstable on exposure to the atmosphere is unusual with the majority of stoichiometric ABO_3 perovskites showing remarkable stability. Consequently we explored the possibility of reducing the rate of decomposition through the use of high pressure-temperature synthesis methods using temperatures from 900 to 1400 ^{o}C and pressures up to 4 GPa. Unfortunately, all these synthesis experiments failed to increase the stability of $BaThO_3$. The reasons for the unusual moisture sensitivity of $BaThO_3$ are not presently understood, although it has been established that actinides dioxides are covered by amorphous hydroxide layers [38]. Nevertheless the instability of $BaThO_3$ may have implications for the stability and storage of other actinides with a perovskite-type lattice such that further studies into the structural chemistry of related transuranic oxides are desirable.

The same high pressure / high temperature method, as well as the conventional solid state method, was also used in attempts to synthesise $SrThO_3$, but without success. The existence of perovskite structured $SrThO_3$ is a debatable point with respect to previous reports. $SrThO_3$, from the Goldschmidt tolerance factor (0.858) perspective, exists on the periphery of the perovskite stability region. Although the formation of $SrThO_3$ in a monoclinic cell was reported, [39] [40, 41] careful examination of the XRD patterns reported in these studies revealed that the patterns are essentially identical to that of the cubic structured ThO_2 in space group $Fm\bar{3}m$.[42] This is consistent with an experimental report by Subasri *et al.* [43] that the solubility of ThO_2 in SrO is limited to 1mol% and the formation of pure ternary phase was not achieved, as well as a theoretical study by Shein *et al.* [27] who predicted, using first-principles calculations, that cubic $SrThO_3$ is unstable with respect to the constituent binary oxides. The latter studies agree well with our failed attempts to synthesise $SrThO_3$ using both the conventional solid state method and the unique high pressure / high temperature route. So the validly of the actual $SrThO_3$ structure formation is questionable, especially considering that the average linear thermal expansion coefficient (1.049×10^{-5} $^{o}C^{-1}$) reported by Purohit *et al.* [41] is very close to our value for ThO_2 (1.01×10^{-5} $^{o}C^{-1}$) and also to other previous ThO_2 investigations. [34, 35]

Conclusions

The room temperature structure of $BaThO_3$ has been refined in orthorhombic *Pbnm* using a combination of S-XRD and NPD data. $BaThO_3$ was observed, for the first time, to undergo a continuous reversible phase transformation to *Ibmm* structural type above 700 ^oC, associated with the loss of the in-phase tilting of the corner sharing ThO_6 octahedra. $BaThO_3$ was observed to decompose upon standing and TGA/DSC and NPD measurements suggest that this is a consequence of reactivity with atmospheric moisture. The volumetric TEC $\bar{\alpha}$ of the *Pbnm* phase is greater than that of the *Ibmm* phase. Attempts to prepare $SrThO_3$ were unsuccessful.

Acknowledgments

This work was, in part, performed at the powder diffraction beamline at the Australian Synchrotron. BJK acknowledges the support of the Australian Research Council and GLM thanks AINSE, and particularly Dr Chris Griffiths and Dr Robert Gee of ANSTO Minerals for their encouragement and continual support for this research.

References

1. L. C. Walters, D. L. Porter and D. C. Crawford, Nuclear fuel considerations for the 21st century, *Progress in Nuclear Energy* **40** (2002), 513-521.
2. P. C. Burns, M. L. Miller and R. C. Ewing, U6+ minerals and inorganic phases: A comparison and hierarchy of crystal structures, *Canadian Mineralogist* **34** (1996), 845-880.
3. R. M. Hazen, R. C. Ewing and D. A. Sverjensky, Evolution of uranium and thorium minerals, *American Mineralogist* **94** (2009), 1293-1311.
4. C. L. Tracy, M. Lang, J. M. Pray, F. Zhang, D. Popov, C. Park, C. Trautmann, M. Bender, D. Severin, V. A. Skuratov and R. C. Ewing, Redox response of actinide materials to highly ionizing radiation, *Nature Communications* **6** (2015), 6133.
5. T. Nakamura, Crystal systems and lattice-constants of perovskite-type compounds $BaThO_3$ and $Ba_2(BaU)O_6$, *Chemistry Letters* **3** (1974), 429-434.
6. Y. Ohishi, E. Yusnitha, K. Kurosaki, H. Muta and S. Yamanaka, Thermophysical properties of $BaThO_3$, *Journal of Nuclear Materials* **448** (2014), 62-65.
7. Y. Hinatsu, The magnetic-susceptibility and structure of $BaUO_3$, *Journal of Solid State Chemistry* **102** (1993), 566-569.
8. G. Murphy, B. J. Kennedy, B. Johannessen, J. A. Kimpton, M. Avdeev, C. S. Griffith, G. J. Thorogood and Z. M. Zhang, Structural studies of the rhombohedral and orthorhombic monouranates: $CaUO_4$, α–$SrUO_4$, β-$SrUO_4$ and BaUO4, *Journal of Solid State Chemistry* **237** (2016), 86-92.

9. A. J. Smith and A. J. E. Welch, Some mixed metal oxides of perovskite structure, *Acta Crystallographica* **13** (1960), 653-656.
10. Y. Harada and S. W. Bradstreet, *Synthesis of refractory mixed oxide with perovskite structure*, Armour Research Foundation, Illinois Insitute of Technology, United States., 1960.
11. G. Murtaza, I. Ahmad, B. Amin, A. Afaq, M. Maqbool, J. Maqssod, I. Khan and M. Zahid, Investigation of structural and optoelectronic properties of BaThO3, *Opt. Mater.* **33** (2011), 553-557.
12. Z. Ali, I. Ahmad and A. H. Reshak, GGA+U studies of the cubic perovskites $BaMO_3$ (M=Pr, Th and U), *Physica B* **410** (2013), 217-221.
13. A. I. Lebedev, Crystal structure and properties of barium thorate $BaThO_3$ from first principles, *Journal of Alloys and Compounds* **580** (2013), 487-490.
14. A. M. Glazer, Classification of tilted octahedra in perovskites, *Acta Crystallographica Section B-Structural Science* **B 28** (1972), 3384-&.
15. C. J. Howard and H. T. Stokes, Group-theoretical analysis of octahedral tilting in perovskites, *Acta Crystallographica Section B-Structural Science* **54** (1998), 782-789.
16. R. V. Krishnan, K. Nagarajan and P. R. V. Rao, Heat capacity measurements on $BaThO_3$ and $BaCeO_3$, *Journal of Nuclear Materials* **299** (2001), 28-31.
17. B. J. Kennedy, C. J. Howard, G. J. Thorogood and J. R. Hester, The influence of composition and temperature on the phases in $Sr_{1-x}Ba_xZrO_3$ perovskites: A high-resolution powder diffraction study, *Journal of Solid State Chemistry* **161** (2001), 106-112.
18. A. K. Prodjosantoso, Q. D. Zhou and B. J. Kennedy, Synchrotron X-ray diffraction study of the $Ba_{1-x}SrSnO_3$ solid solution, *Journal of Solid State Chemistry* **200** (2013), 241-245.
19. C. J. Howard, K. S. Knight, B. J. Kennedy and E. H. Kisi, The structural phase transitions in strontium zirconate revisited, *Journal of Physics-Condensed Matter* **12** (2000), L677-L683.
20. B. J. Kennedy, B. A. Hunter and J. R. Hester, Synchrotron x-ray diffraction reexamination of the sequence of high-temperature phases in $SrRuO_3$, *Physical Review B* **65** (2002), 4.
21. E. E. Rodriguez, F. Poineau, A. Llobet, B. J. Kennedy, M. Avdeev, G. J. Thorogood, M. L. Carter, R. Seshadri, D. J. Singh and A. K. Cheetham, High Temperature Magnetic Ordering in the 4d Perovskite $SrTcO_3$, *Physical Review Letters* **106** (2011), 4.
22. G. J. Thorogood, M. Avdeev, M. L. Carter, B. J. Kennedy, J. Ting and K. S. Wallwork, Structural phase transitions and magnetic order in $SrTcO_3$, *Dalton Transactions* **40** (2011), 7228-7233.
23. N. R. Brown, J. J. Powers, B. Feng, F. Heidet, N. E. Stauff, G. Zhang, M. Todosow, A. Worrall, J. C. Gehin, T. K. Kim and T. A. Taiwo, Sustainable thorium nuclear fuel cycles: A comparison of intermediate and fast neutron spectrum systems, *Nuclear Engineering and Design* **289** (2015), 252-265.
24. D. J. Gregg, Z. M. Zhang, G. J. Thorogood, B. J. Kennedy, J. A. Kimpton, G. J. Griffiths, P. R. Guagliardo, G. R. Lumpkin and E. R. Vance, Cation antisite disorder in uranium-doped gadolinium zirconate pyrochlores, *Journal of Nuclear Materials* **452** (2014), 474-478.
25. G. L. Murphy, B. J. Kennedy, J. A. Kimpton, Q. F. Gu, B. Johannessen, G. Beridze, P. M. Kowalski, D. Bosbach, M. Avdeev and Z. M. Zhang, Nonstoichiometry in strontium uranium oxide: Understanding the rhombohedral-orthorhombic transition in $SrUO_4$, *Inorganic Chemistry* **55** (2016), 9329-9334.
26. E. Reynolds, B. J. Kennedy, M. Avdeev, G. J. Thorogood, Z. M. Zhang and H. E. A. Brand, Structural and spectroscopic studies of $Ba_2Y_{1-d}UO_{6+x}$, *Journal of Solid State Chemistry* **243** (2016), 8-11.
27. I. R. Shein, K. I. Shein and A. L. Ivanovskii, Elastic and electronic properties and stability of $SrThO_3$, $SrZrO_3$ and ThO_2 from first principles, *Journal of Nuclear Materials* **361** (2007), 69-77.
28. K. S. Wallwork, B. J. Kennedy and D. Wang, The high resolution powder diffraction beamline for the Australian Synchrotron, *AIP Conference Proceedings* **879** (2007), 879-882.

29. K.-D. Liss, B. Hunter, M. Hagen, T. Noakes and S. Kennedy, Echidna - the new high-resolution powder diffractometer being built at OPAL, *Physica B* **385-86** (2006), 1010-1012.
30. A. C. Larson and R. B. Von Dreele, GSAS, *General Structure Analysis System. LANSCE, MS-H805, Los Alamos, New Mexico*(1994).
31. B. H. Toby, EXPGUI, a graphical user interface for GSAS, *J. Appl. Crystallogr.* **34** (2001), 210-213.
32. G. Wallez, N. Clavier, N. Dacheux and D. Bregiroux, Negative thermal expansion in $Th_2O(PO_4)_2$, *Materials Research Bulletin* **46** (2011), 1777-1780.
33. B. K. Greve, K. L. Martin, P. L. Lee, P. J. Chupas, K. W. Chapman and A. P. Wilkinson, Pronounced Negative Thermal Expansion from a Simple Structure: Cubic ScF_3, *Journal of the American Chemical Society* **132** (2010), 15496-15498.
34. A. C. Momin, E. B. Mirza and M. D. Mathews, High-temperature x-ray diffractometric studies on the lattice thermal-expansion behavior of UO_2, ThO_2 and $(U_{0.2}Th_{0.8})O_2$ doped with fission-product oxides, *Journal of Nuclear Materials* **185** (1991), 308-310.
35. T. Yamashita, N. Nitani, T. Tsuji and H. Inagaki, Thermal expansions of NpO_2 and some other actinide dioxides, *Journal of Nuclear Materials* **245** (1997), 72-78.
36. R. B. Roberts and G. K. White, Thermal expansion of fluorites at high temperatures, *Journal of Physics C: Solid State Physics* **19** (1986), 7167.
37. R. Mishra, M. Ali, S. R. Bharadwaj, A. S. Kerkar, D. Das and S. R. Dharwadkar, Thermodynamic stability of barium thorate, $BaThO_3$, from a Knudsen effusion study, *Journal of Alloys and Compounds* **290** (1999), 97-102.
38. V. Neck and J. I. Kim, Solubility and hydrolysis of tetravalent actinides, *Radiochimica Acta* **89** (2001), 1-16.
39. M. Ali, R. Mishra, S. R. Bharadwaj, A. S. Kerkar, S. R. Dharwadkar and D. Das, Thermodynamic stability of solid $SrThO_3$, *Journal of Nuclear Materials* **299** (2001), 165-170.
40. R. Prasad, S. Dash, S. C. Parida, Z. Singh and V. Venugopal, Thermodynamic studies on $SrThO_3$(S), *Journal of Nuclear Materials* **312** (2003), 1-9.
41. R. D. Purohit, A. K. Tyagi, M. D. Mathews and S. Saha, Combustion synthesis and bulk thermal expansion studies of Ba and Sr thorates, *Journal of Nuclear Materials* **280** (2000), 51-55.
42. I. C. Cosentino and R. Muccillo, Lattice parameters of thoria-yttria solid solutions, *Materials Letters* **48** (2001), 253-257.
43. R. Subasri, C. Mallika, T. Mathews, V. S. Sastry and O. M. Sreedharan, Solubility studies, thermodynamics and electrical conductivity in the $Th_{1-x}Sr_xO_2$ system, *Journal of Nuclear Materials* **312** (2003), 249-256.